1
2
3
4
5

Vaccine-elicited murine antibody WS6 neutralizes diverse beta-coronaviruses by recognizing a helical stem supersite of vulnerability

Wei Shi[1,3], Lingshu Wang[1,3], Tongqing Zhou[1,3], Mallika Sastry[1], Eun Sung Yang[1], Yi Zhang[1], Man Chen[1], Xuejun Chen[1], Misook Choe[1], Adrian Creanga[1], Kwan Leung[1], Adam S. Olia[1], Amarendra Pegu[1], Reda Rawi[1], Chen-Hsiang Shen[1], Erik-Stephane D. Stancofski[1], Chloe Adrienna Talana[1], I-Ting Teng[1], Shuishu Wang[1], Kizzmekia S. Corbett[1], Yaroslav Tsybovsky[2], John R. Mascola[1*], Peter D. Kwong[1,4*]

[1] Vaccine Research Center, National Institute of Allergy and Infectious Diseases, National Institutes of Health, Bethesda, MD 20892, USA

[2] Electron Microscopy Laboratory, Cancer Research Technology Program, Leidos Biomedical Research, Inc., Frederick National Laboratory for Cancer Research, Frederick, MD 21702, USA.

[3] These authors contributed equally
[4] Lead Contact

* Correspondence: jmascola@nih.gov (J.R.M.), pdkwong@nih.gov (P.D.K.)

30

31

32

Summary

Immunization with SARS-CoV-2 spike elicits diverse antibodies, but can any of these neutralize broadly? Here, we report the isolation and characterization of antibody WS6, from a mouse immunized with mRNA encoding the SARS-CoV-2 spike. WS6 bound diverse beta-coronavirus spikes and neutralized SARS-CoV-2 variants, SARS-CoV, and related sarbecoviruses. Epitope mapping revealed WS6 to target a region in the S2 subunit, which was conserved among SARS-CoV-2, MERS-CoV, and hCoV-OC43. The crystal structure at 2-Å resolution of WS6 with its S2 epitope revealed recognition to center on a conserved helix, which was occluded in both prefusion and post-fusion spike conformations. Structural and neutralization analyses indicated WS6 to neutralize by inhibiting fusion, post-viral attachment. Comparison of WS6 to other antibodies recently identified from convalescent donors or mice immunized with diverse spikes indicated a stem-helical supersite – centered on hydrophobic residues Phe1148, Leu1152, Tyr1155, and Phe1156 – to be a promising target for vaccine design.

46

47

Highlights

- SARS-CoV-2 spike mRNA-immunized mouse elicited an antibody, WS6, that cross reacts with spikes of diverse human and bat beta-coronaviruses

- WS6 neutralizes SARS-CoV-2 variants, SARS-CoV, and related viruses

- Crystal structure at 2-Å resolution of WS6 in complex with a conserved S2 peptide reveals recognition of a helical epitope

- WS6 neutralizes by inhibition of fusion, post-viral attachment

- WS6 recognizes a supersite of vulnerability also recognized by other recently identified antibodies

- Helical supersite of vulnerability comprises a hydrophobic cluster spanning three helical turns, with acid residues framing the center turn

- Genetic and structural analysis indicate supersite recognition to be compatible with diverse antibody ontogenies

Introduction

The COVID-19 pandemic, resulting from the zoonotic infection of severe acute respiratory syndrome coronavirus 2 (SARS-CoV-2), continues to rage on, fueled by continuously evolving variants, which are making current licensed vaccines less effective (Araf et al., 2022; Doria-Rose et al., 2021; Edara et al., 2021; Garcia-Beltran et al., 2022; Liu et al., 2021). Vaccines capable of neutralizing all SARS-CoV-2 variants for the foreseeable future are of high interest. Antibodies with broad neutralizing capacity are also of interest: if ultrapotent, they might be useful as therapeutic antibodies; but even if only moderate potency, their epitopes are useful as vaccine templates (Kong et al., 2016).

Virtually all neutralizing antibodies are directed against the trimeric ectodomain of the spike glycoprotein, which comprises two subunits S1 and S2. Neutralizing antibodies isolated from COVID-19 convalescent donors or from vaccinees after spike immunization are directed primarily against the N-terminal domain (NTD) or receptor-binding domain (RBD) on the S1 subunit of the trimeric viral surface spike glycoprotein (Spike) (Barnes et al., 2020; Brouwer et al., 2020; Cao et al., 2020; Cerutti et al., 2021; Ju et al., 2020; Liu et al., 2020; McCallum et al., 2021; Robbiani et al., 2020; Rogers et al., 2020; Seydoux et al., 2020; Suryadevara et al., 2021; Zost et al., 2020). Evolving SARS-CoV-2 variants, such as Delta and Omicron, evade these antibodies by mutations that reduce or knockout antibody binding, but maintain or even enhance infectivity (Garcia-Beltran et al., 2022; Liu et al., 2021; Sievers et al., 2022; Syed et al., 2022). Antibodies against most other regions on the spike are generally poorly neutralizing to non-neutralizing; several antibodies, however, such as antibody S2P6 (Pinto et al., 2021) have been reported to neutralize diverse strains of beta coronaviruses through recognition of a stem-helix supersite of vulnerability in the S2 subunit (Hsieh et al., 2021; Li et al., 2022; Sauer et al., 2021; Zhou et al., 2021).

4

86   To investigate the breadth of neutralizing antibodies obtained from mice vaccinated by

87   mRNA encoding the SARS-CoV-2 spike, we assessed monoclonal antibodies for the location of

88   their epitopes, the breadth of their binding to diverse spikes, and their neutralization capacities. We

89   found one, antibody WS6, with broad binding capacity and moderate neutralization potency, and

90   we determined its crystal structure in complex with its epitope, the step in the entry pathway where

91   it neutralized, and how its recognition compared with other recently identified antibodies with

92   overlapping epitopes. The results reveal a highly promising vaccine target in the S2 subunit –

93   comprising a hydrophobic cluster spanning three helical turns, with acidic residues framing its

94   center turn – and add WS6 to the panel of antibodies by which to guide its vaccine development.

95

96   **Results**

97   **Identification and characterization of SARS-CoV-2 spike-specific antibodies from**

98   **immunized mice**

99   To obtain antibodies specific for SARS-CoV-2 spike glycoprotein, we immunized mice

100   with mRNA coding for SARS-CoV-2 spike (**Figure 1A**). To generate hybridomas, we boosted

101   with soluble spike protein and after three days generated hybridomas by fusing splenocyte B cells

102   with Sp2/0 cells from the mouse with the highest plasma neutralization titers to SARS-CoV-2.

103   Eleven monoclonal antibodies, named WS1 to WS11, bound SARS-CoV-2 S-dTM by ELISA

104   (**Figure 1B**). Nine of these bound the S1 subunit, either S1-short1 (spike residues 1-670) or S1R

105   (residues 1-537). Six of them, WS1, WS2, WS3, WS7, WS8, and WS10, bound NTD; and three of

106   them, WS4, WS9, and WS11, bound RBD. Antibodies WS5 and WS6, however, did not bind

107   NTD, RBD, or S1, and their binding epitopes were presumably on the S2 subunit of the spike.

108   To provide insight into the breadth of binding, we assessed recognition of WS1-11 on a

109   panel of prefusion-stabilized diverse beta-coronavirus spikes (S2Ps) (Wrapp et al., 2020).

110   Detectable binding was observed against SARS-CoV-2, SARS-CoV, MERS-CoV and hCoV-

111   HKU1 for five antibodies (**Figure 1C**). For antibodies WS3, WS4, and WS7, binding was more

112   than 1,000-times weaker against the divergent strain versus that of the immunogen. However, for

113   antibodies WS5 and WS6, binding was only about 10-fold reduced versus SARS-CoV-2.

114   Neutralization assessments revealed that WS5 neutralized neither SARS-CoV-2 nor SARS-CoV,

115   whereas WS6 could neutralize both (**Figure 1D**). WS6 was further studied for its epitope and

116   neutralization activities.

117

118   **WS6 recognizes diverse beta-coronaviruses spikes and neutralizes SARS-CoV-2 and**

119   **variants, SARS-CoV, and related viruses from bat, pangolin, and other animals**

120   To assess fully the broad reactivity of WS6, we performed ELISAs against S2Ps from an

121   even more divergent panel of coronaviruses, including RaTG13, WIV1, SHC014, hCoV-OC43,

122   and hCoV-229E (**Figure 2A**). Remarkably, WS6 was able to bind all beta-coronaviruses tested,

123   though not to the alpha-coronavirus hCoV-229E (**Figure S1**). The apparent binding affinities of

124   WS6 to S2Ps, measured by biolayer interferometry (BLI), showed nanomolar or lower dissociation

125   constants (K_{DS}), with slow dissociation such that k_{off} values could not be determined accurately in

126   many cases (**Figure 2B**). To determine if WS6 could bind spike proteins on cell surface, we

127   expressed spikes of SARS-CoV-2, SARS-CoV, MERS-CoV, hCoV-HKU1, and hCoV-OC43 on

128   the surface of Expi-293 cells and analyzed WS6 binding by flow cytometry. We found that WS6

129   bound well to the cell surface expressing the beta-coronavirus spikes (**Figures 2C and S2**).

130   To determine if the broad recognition of WS6 for spikes translated into broad neutralization

131 of beta-coronaviruses, we assessed its neutralization activities by pseudovirus neutralization assays

132 (Naldini et al., 1996; Wang et al., 2021). WS6 neutralized all tested variants of SARS-CoV-2

133 including Omicron (B.1.1.529), with IC_{50} 2.46-26.52 µg/ml (**Figures 2D and S3; Table S1**). WS6

134 could also neutralize beta-coronaviruses related to SARS-CoV-2 (such as RaTG13, Pangolin_GD,

135 and Pangolin_GX), SARS-CoV, and related viruses Frankfurt1, Civet007-2004, WIV1, and

136 SHC014 with IC_{50} 0.11-4.91 µg/ml (**Figures 2D and S3; Table S1**). WS6 also neutralized related

137 beta-coronaviruses, such as RaTG13, Pangolin-GX, Civet007-2004, and SHC014, with sub

138 micromolar IC_{50}, better than against SARS-CoV-2 despite being elicited by immunizations with

139 SARS-CoV-2 spike. The only tested beta-coronavirus strain WS6 failed to neutralize was MERS-

140 CoV, consistent with its lower ELISA binding to this strain (**Table S1**).

141

142 **WS6 epitope mapping**

143   We attempted to map the epitope of WS6 by visualizing its recognition of the spike

144 ectodomain by negative strain-electron microscopy (EM). 2D-classification of antigen-binding

145 fragment (Fab) of WS6 in complex with the S2P spike (WA-1 strain) showed generally unbound

146 spikes, with only 4% of the images yielding a trimer with Fabs binding in the membrane-proximal

147 S2 stem (**Figure 3A**). We also analyzed Fab WS6 in complex with spike S2 subunit; 2D-

148 classification indicated WS6 to bind S2, though most of S2 appeared to be disordered (**Figure 3B**).

149   To further map the epitope, we performed peptide array-based epitope mapping and

150 identified a 17-residue peptide, PELDSFKEELDKYFKNH (SARS-CoV-2 spike residues 1143-

151 1159) to bind WS6 (**Figure 3C**), suggesting WS6 epitope to be at the S2 stem-helix region of the

152 spike near the viral membrane, consistent with our negative stain-EM observation. This peptide is

7

153   conserved among SARS-CoV, SARS-CoV-2, and RaTG13, and is mostly conserved among

154   diverse beta-coronaviruses (**Figure S4A**).

155

156   **Crystal structure of WS6 in complex with a conserved S2 peptide**

157   To elucidate the mechanism for the broad reactivity of WS6, we determined a crystal

158   structure at 2 Å of Fab WS6 in complex with peptide Ace-F_{1148}KEELDKYFK$_{1157}$-PEG12-Lys-

159   Biotin (residue numbers were based on the SARS-CoV-2 spike sequence) (**Figure 3D and Table**

160   **S2**). The peptide contained a 10-residue segment conserved among beta-coronaviruses (**Figure S4A**)

161   and was acetylated at N terminus and biotin-pegylated at C terminus. Well-defined electron density

162   was observed for the entire WS6 Fab and for the entire peptide, including the acetyl group at the N

163   terminus and part of the polyethylene glycol at the C terminus (**Figure 3D**). Peptide binding

164   interactions involved both heavy and light chains, with heavy chain contributing ~360 Å^2 buried

165   surface area (BSA) and light chain contributing ~230 Å^2 (**Table S3**). The BSA of the peptide was

166   slightly larger at ~675 Å^2, not counting the BSA of the visible PEG fragment (~100 Å^2 total). This

167   binding interface is smaller than a typical antibody-binding epitope, indicating the full WS6 epitope

168   to likely involve additional residues.

169   All complementarity-determining regions (CDRs) of both heavy and light chains were

170   involved in binding, creating a groove that cradled the epitope (**Figure 3D**). In the WS6-bound

171   crystal structure, the S2 epitope formed a three-turn α helix; examination of its binding mode

172   revealed binding for a longer helix with extensions on both termini without any major clashes. Most

173   of the residues of the peptide involved in binding, except for Glu1150 and Lys1154, which were on

174   the side of the helix facing WS6 (**Figure 3E**). Aromatic or hydrophobic residues, Phe1148,

175   Leu1152, Tyr1155, and Phe1156, were on the side of the helix facing WS6. Phe1148 had aromatic

8

176   interactions with $Arg50_L$ and $Tyr91_L$ of WS6 light chain and hydrophobic interactions with $Ser97_H$

177   of heavy chain. Tyr1155 side chain stuck into a cavity form by CDR L3 from $Tyr91_L$ to $Pro96_L$ and

178   had aromatic or hydrophobic interactions with side chains of $Tyr91_L$, $Tyr94_L$, and $Pro96_L$ and the

179   peptide backbone. Leu1152 and Phe1156 side chains bound in a pocket between heavy and light

180   chains and interacted with side chains of $Tyr91_L$, $Pro96_L$, $Phe99_H$, $Thr95_H$, $Trp33_H$, $His35_H$, and

181   $Tyr47_H$ (**Figure 3E and 3F and Table S3**).

182

183   **WS6 neutralizes by inhibition of fusion steps post viral attachment**

184   To elucidate the mechanism by which WS6 neutralize beta-coronaviruses, we incubated

185   BHK21-ACE2 cells with SARS-CoV-2 spike pseudotyped lentivirus on ice to allow virus to attach

186   to ACE2. After thorough washing, cells were incubated with WS6 or WS4 on ice for one hour and at

187   37 □ for 72 hours. WS4, an RBD-directed neutralizing antibody, could neutralize not more than

188   40% of the virus, whereas WS6 had no problem neutralizing the ACE2 pre-attached virus (**Figure**

189   **4A**). We performed a similar experiment using 293 flpin-TMPRSS2-ACE2 cells for WS6 and S2P6

190   (Pinto et al., 2021), which also binds to the S2-stem helix, and found that both antibodies could

191   neutralize ACE2 pre-attached virus. These results suggest that WS6 is likely to neutralize SARS-

192   CoV-2 by engaging in steps post-viral attachment to ACE2.

193   As described above in the structural analysis, WS6 recognized the hydrophobic face of the

194   stem helix with residues Phe1148, Leu1152, Tyr1155, and Phe1156 binding in the center of the

195   paratope groove. In the prefusion structure of SARS-CoV-2 spike (PDB: 6xr8) (Cai et al., 2020; Ke

196   et al., 2020), these hydrophobic side chains pack in the coiled-coil interface of the 3-helical bundle.

197   Modeling of WS6 binding to the prefusion SARS-CoV-2 spike, based on the WS6-peptide complex,

198   revealed substantial clashes (**Figure 4B, left panel**), indicating that WS6 binding would require

9

199   unpacking or disassembly of the helical bundle. Similarly, the postfusion spike structure (PDB: 6xra)

200   (Cai et al., 2020) was incompatible with binding of WS6 to the hydrophobic side of the peptide helix

201   as revealed by the crystal structure, because these hydrophobic residues are involved in the packing

202   of the small helix with the central coiled coil in the postfusion structure (**Figure 4B, right panel**).

203   Because the spike binding to the receptor and transitioning from the prefusion conformation to

204   postfusion conformation drive the membrane fusion process, WS6 maybe even more apt to bind

205   during this conformational transition and inhibit the fusion process (**Figure 4C**).

206

207   **A helical stem supersite of vulnerability**

208   Several broad beta-coronavirus-neutralizing antibodies have been identified recently that

209   target the S2 stem-helix region, including the afore mentioned S2P6 (Pinto et al., 2021) as well as

210   antibodies B6 (Sauer et al., 2021), IgG22 (Hsieh et al., 2021), CCP40.8 (Zhou et al., 2021), and

211   CV3-25 (Li et al., 2022). Superposition of their S2 helical epitopes indicated these antibodies to

212   bind to the stem helix with varying orientations (**Figure 5A**) and to target different sets of residues

213   ranging from residue position 1142 to 1164 on S2 (**Figures 5B and S5**). Epitope analysis indicated

214   a common subset of residues, namely Phe1148, Lys1149, Glu1153, Leu1152, Asp1153, Tyr1155,

215   and Phe1156, to interact with four of the six antibodies (**Figure 5B, left**). These residues, which

216   spanned three helical turns on S2 with a central hydrophobic cluster sandwiched by hydrophilic

217   residues Lys1149, Glu1151, and Asp1153, formed a supersite of vulnerability for antibody

218   recognition (**Figure 5B, middle and right**). Sequence analysis indicated this S2 supersite to be

219   highly conserved among beta-coronaviruses (**Figure 5C**), providing the basis for the broad

220   neutralization by WS6 and other antibodies targeting this site. Overall, these S2 stem-helix

221   antibodies are likely to share a similar mechanism of neutralization. Before or even after spike

10

222   binds to ACE2, the stem helix appears to adopt a conformation or conformations that expose this

223   supersite, allowing for the stem-helix antibodies to bind and prevent spike conformations needed

224   for fusion, thereby stalling the entry process. Importantly, these S2-helix directed broad neutralizers

225   have diverse origin genes, except for B6 and IgG22, which utilize the same VH gene and appears to

226   be of the same antibody class (Figure S4B). In addition, the antibodies have only low-to-moderate

227   somatic hypermutation, suggesting diverse ontogenies are possible with little barrier to their

228   development **(Figure S4)**.

229

230   **Discussion**

231   Zoonotic infections from beta-coronaviruses have caused multiple pandemics and endemics

232   in recent years, including SARS (Drosten et al., 2003; Ksiazek et al., 2003), Middle East

233   respiratory syndrome (MERS) (Zaki et al., 2012), and the ongoing COVID-19 (Zhou et al., 2020a;

234   Zhu et al., 2020). It seems likely that additional beta-coronavirus zoonotic pandemics will occur in

235   the future. Broadly neutralizing antibodies or broad vaccines against a wide spectrum of beta-

236   coronaviruses may be effective at preventing or ameliorating such pandemics – and could even be

237   of use against the current COVID-19, if variants do succeed in escape control by current vaccines.

238   In this study, we isolated an S2-directed antibody, named WS6, from a mouse immunized with

239   mRNA-encoded SARS-CoV-2 spike. WS6 could bind and neutralize all variants of SARS-CoV-2,

240   including Delta and Omicron; it could also neutralize SARS-CoV, as well as bat, civet, and

241   pangolin beta-coronaviruses related to SARS-CoV and SARS-CoV-2. Crystal structure of WS6 in

242   complex with S2 stem-helix epitope peptide revealed the structural basis for broad recognition and,

243   together with neutralization and binding analyses, suggest a potential mechanism by which WS6

244   neutralize broadly beta-coronaviruses.

245   Several other groups have recently reported S2-directed antibodies including antibodies

246   S2P6 (Pinto et al., 2021), CC40.8 (Zhou et al., 2021) and CV3-25 (Li et al., 2022) from SARS-

247   CoV-2-infected convalescent donors and B6 (Sauer et al., 2021) and IgG22 (Hsieh et al., 2021)

248   from vaccinated mice. We measured directly the neutralization of both WS6 and S2P6 to diverse

249   SARS-CoV-2 variants and to diverse coronaviruses generally (**Figure S3**). In light of its high

250   breadth, we were surprised to find S2P6 was unable to neutralize the Omicron variant of SARS-

251   CoV-2, although WS6 did neutralize Omicron. WS6 did, however, neutralize all tested strains

252   more potently than S2P6, except for MERS-CoV, against which WS6 was non-neutralizing. In

253   terms of the murine antibodies, the recognition of antibodies B6 and IgG22 was very similar, both

254   utilizing the same heavy chain origin gene (VH1-19) and both generated after immunization with

255   spikes from SARS-CoV-2 and MERS-CoV (Hsieh et al., 2021; Pinto et al., 2021). By contrast,

256   WS6 did not use the same V-gene and was generated only by immunization with the SARS-CoV-2

257   spike – thereby revealing a new mode of murine S2-helix recognition and showing MERS-CoV

258   spike immunization was no required to elicit these antibodies.

259   It will be interesting to determine whether S2-helix peptide-based immunizations can focus

260   the immune response, enabling the elicitation of broadly neutralizing serological responses, as has

261   been done with HIV-1 fusion peptide (Kong et al., 2019; Xu et al., 2018). Nanoparticles displaying

262   the S2-helix may also be helpful in focusing the immune response, as has been done with the

263   influenza stem cite of vulnerability (Boyoglu-Barnum et al., 2021; Kanekiyo et al., 2013; Yassine

264   et al., 2015). Whether S2-helix focused immunization will enable sufficiently broad and potent

265   responses to enable protection from future SARS-CoV-2 variants or to future beta-coronavirus

266   zoonotic crossovers remains to be seen. It seems likely that such immune focusing can be carried

267   out in conjunction with spike-based immunizations, perhaps using currently licensed vaccines

268   from Moderna, Pfizer and Johnson and Johnson, all of which incorporate the S2-helical region.

269

Acknowledgements

281

Author Contributions

283   W.S. isolated antibodies WS1-WS11 and performed ELISA binding assays; L.W. headed

284   neutralization studies, prepared spike plasmids and performed cell surface binding assays; T.Z.

285   determined and analyzed the crystal structure of WS6-peptide complex, and wrote manuscript;

286   M.S. performed Octet binding assays, provided spike proteins for ELISA, and assisted with

287   obtaining peptide for crystallization; E.S.Y., Y.Z., and M.Chen performed WS6 neutralization of

288   SARS related viruses; X.C. provided mouse NGS sequence data; M.Choe provided S2P6 antibody;

289   A.C. provided 293 flpin-TMPRSS2-ACE2 cells; K.L. assisted with preparation of pseudoviruses;

13

290   A.S.O provided SARS-CoV-2 S2P-His for Octet measurements; A.P. and C.A.T performed cell

291   surface staining; R.R. assisted with obtaining Peptide for crystallization; C.-H.S. prepared

292   phylogenetic tree; E.-S.S. crystallized the protein complex; I.-T.T. performed transfection for Beta-

293   CoV and S2 antibody productions; S.W. wrote manuscript and performed PISA analysis of

294   antibody-peptide interface; K.S.C carried out mouse immunization experiment; Y.T. performed

295   negative-stain EM analysis; J.R.M. supervised antibody isolation, neutralization assessments, and

296   cell surface binding assays; P.D.K. oversaw the project and - with S.W and T.Z - wrote the

297   manuscript, with all authors providing comments or revisions.

298

299   **Competing interest declaration**

300   The authors declare no competing interest.

301

302

303 **METHODS**

304 **RESOURCE AVAILABILITY**

305 **Materials Availability**

306 Plasmids generated in this study are available upon request.

307

308 **Data and Code Availability**

309 Crystal diffraction data and structure coordinates of WS6 in complex have been deposited with the

310 Protein Data Bank, PDB: 7TCQ, DOI: 10.2210/pdb7tcq/pdb.

311

312 **EXPERIMENTAL MODEL AND SUBJECT DETAILS**

313 **Mouse Studies**

314   Animal experiments were carried out in compliance with all pertinent US National

315 Institutes of Health regulations and approval from the Animal Care and Use Committee (ACUC)

316 of the Vaccine Research Center. BALB/cJ mice (Jackson Laboratory), 6- to 8-week-old female,

317 were used.

318

319 **Cell Lines**

320   FreeStyle 293-F (cat# R79007) and Expi293F cells (cat# A14528; RRID: CVCL_D615)

321 were purchased from ThermoFisher Scientific Inc. FreeStyle 293-F cells were maintained in

322 FreeStyle 293 Expression Medium, while Expi293F cells were maintained in Expi Expression

323 Medium. The above cell lines were used directly from the commercial sources and cultured

324 according to manufacturer suggestions.

325

326   **METHOD DETAILS**

327   **Mouse immunization, hybridoma generation and mAb isolation**

328   Mice were immunized with mRNA coding for SARS-CoV-2 spike of the wildtype WA-1 strain at

329   weeks 0 and 3 intramuscularly, utilizing methods described previously (Corbett et al., 2020). One

330   mouse with the best neutralizing antibody titer against SARS-CoV-2 spike was boosted

331   intravenously with 20 μg of SARS-CoV-2 S-dTM at week 12. Three days later, splenocytes were

332   harvested and fused with Sp2/0 myeloma cells (ATCC) using polyethylene glycol (PEG) 1450

333   (50% (w/v), Sigma-Aldrich) according to the standard methods. Cells were cultured and screened

334   in RPMI complete medium that contained 20% FCS and 1×100 μM hypoxanthine, 0.4 μM

335   aminopterin and 16 μM thymidine (Sigma-Aldrich). Supernatants from resulting hybridomas

336   were screened for binding, using ELISA, to SARS-CoV-2- S1, NTD, RBD or S-dTM as well as

337   for neutralizing activity. Subclones were generated by limiting dilution. After three rounds of

338   screening and subcloning, stable antibody-producing clones were isolated and adapted to

339   hybridoma-serum-free medium (Life Technologies Corp., Grand Island, NY, USA). Supernatants

340   were collected from selected hybridoma clones and purified through a protein G-sepharose column

341   (GE Healthcare). mAbs were isotyped with Pierce rapid isotyping kit (Cat#26178). mAb Fabs

342   were generated using Pierce Fab kit (Cat#44985) following manufacturer's instructions. mAb and

343   Fab purity was confirmed by SDS-PAGE. Selected hybridoma were sent to GenScript

344   (Piscataway, NJ 08854, USA) for hybridoma heavy and light chain variable sequences and IMGT

345   analysis.

346

347   **ELISA and dot-blot**

16

348   ELISA plates were coated with the SARS-CoV-2 proteins, S-dTM, S1-short (residues 1-670), S1R

349   (residues 1-537), RBD, and NTD, at 1 μg/ml in PBS at 4 °C overnight. After standard washes

350   and blocks, plates were incubated with 50ul/each well, serial dilutions of mAbs for one hour at

351   room temperature. Anti-mouse whole IgG horseradish peroxidase conjugates (Jackson Laboratory)

352   were used as secondary antibodies, and 3,5,3′5′-tetramethylbenzidine (TMB) (KPL, Gaithersburg,

353   MD) was used as the substrate.

354   To identify WS6 epitope, a dot-blot was performed. SARS-CoV spike peptide array (NR-

355   52418), was purchased from BEI resource. Seventy-eight peptides (#91-169) from the peptide

356   array which covers SARS-CoV spike S2 region, were dotted on a nitrocellulose membrane

357   respectively, 20ng/2ul/each dot. SARS-CoV-2 RBD, S2, S-dTM and S2P proteins were also dotted

358   on the membrane as controls. Block non-specific sites by soaking in 5% dry milk in PBS-Tween

359   20. The membrane was washed three times with PBS-T buffer, then incubated with 2ug/ml of

360   mAb, WS6 in blocking buffer for one hour at room temperature. After wash three times with PBS-

361   T buffer, the membrane was incubated half hour with anti-mouse IgG horseradish peroxidase

362   conjugates (Jackson Laboratory) as secondary antibody. Then membrane was developed with ECL

363   medium.

364

365   **Expression and purification of beta-coronavirus spike trimer proteins**

366   Diverse beta-coronavirus spike soluble proteins were stabilized in prefusion conformation by

367   double-proline mutations corresponding to K986P and V987P in SARS CoV-2 spike protein, along

368   with a T4-phage fibritin trimerization domain (foldon) at the C terminus (Wrapp et al., 2020)

369   followed by an HRV3C cleavage site, His8 and Twin-Streptactin purification tags. Additionally,

370   the furin cleavage sites between S1 and S2 were mutated; for HKU1 and OC43, RRKRR was

371 replaced by GGSGG; for MERS-CoV, RSVR was replaced with ASVG; for SARS-CoV, SHC014,

372 WIV1, and RaTG13, SLLRST was replaced with SLLAST. DNA sequences encoding diverse

373 beta-coronavirus S2P proteins were cloned into mammalian expression vector pVRC8400 and the

374 proteins expressed by transient transfection of FreeStyle 293-F cells as previously described (Zhou

375 et al., 2020b). Specifically, 1 mg of transfection grade plasmid DNA and 3 ml of Turbo293

376 transfection reagent (Speed BioSystems) each in 20ml Opti-MEM (Thermo Fisher Scientific),

377 were pre-mixed and transfected into FreeStyle 293-F cells. Transfected cells were grown for 6

378 days at 37 °C, and the supernatant was harvested by centrifugation to remove cell debris.

379 Supernatants were sterile-filtered, and the spike trimers were purified by nickel affinity

380 chromatography using cOmplete His-Tag purification resin. The resin was washed with 50 mM

381 Tris, 400 mM NaCl, 10 mM and 25 mM Imidazole pH 8.0 buffer. The proteins were eluted in 50

382 mM Tris pH 8.0, 400 mM NaCl, 300 mM Imidazole. Protein fractions were pooled and further

383 purified by size-exclusion chromatography (SEC) using a Superdex 200 16/600 column (Cytiva) in

384 PBS. Fractions corresponding to trimeric spike proteins were pooled, concentrated to 1 mg/ml.

385

Production of antibodies

387 Antibody heavy and light variable region gene sequences were synthesized (Gene Universal Inc,

388 Newark DE) and subcloned into corresponding pVRC8400 vectors (https://www.addgene.org).

389 The resulting plasmids of heavy and light chain pairs were co-transfected in Expi293F cells

390 (Thermo Fisher) using Turbo293 transfection reagent (Speed BioSystems) as described previously

391 (Wu et al., 2011). On day 6 post transfection, the culture supernatants were harvested, sterile

392 filtered and loaded onto a protein A column. The columns were washed with PBS, and IgG

393 proteins were eluted with a low pH IgG elution buffer (Pierce) and immediately neutralized with

18

394   1M Tris-HCl pH 8.0. Purified IgGs were subsequently dialyzed twice against PBS pH 7.4 using 10

395   kD dialysis cartridges (Pierce) and used for measurements.

396

Full-length spike constructs

398   Codon optimized cDNAs encoding full-length spike from SARS-CoV-2 (GenBank ID:

399   QHD43416.1) were synthesized, cloned into the mammalian expression vector VRC8400

400   (Barouch et al., 2005) and confirmed by sequencing. Spike containing D614G amino acid change

401   was generated using the wildtype spike sequence. Other variants containing single or multiple

402   amino-acid changes in the spike gene from wildtype or D614G were made by mutagenesis using

403   QuickChange lightning Multi Site-Directed Mutagenesis Kit (cat # 210515, Agilent) or via

404   synthesis and cloning (Genscript). The spike variants tested are B.1.1.7 (H69del-V70del-Y144del-

405   N501Y-A570D-D614G-P681H-T716I-S982A-D1118H), B.1.351 (L18F-D80A-D215G-(L242-

406   244)del-R246I-K417N-E484K-N501Y-A701V), P.1 (L18F-T20N-P26S-D138Y-R190S-K417T-

407   E484K-N501Y-D614G-H655Y-T1027I-V1176F), B.1.617.2 (T19R, G142D, del156-157, R158G,

408   L452R, T478K, D614G, P681R, D950N), AY.1 (T19R, T95I, G142D, E156del, F157del, R158G,

409   W258L, K417N, L452R, T478K, D614G, P681R, D950N), B.1.621 (T95I, insert144T, Y144S,

410   Y145N, R346K, E484K, N501Y, D614G, P681H, D950N) and B.1.1.529 (A67V, H69del,

411   V70del, T95I, G142D, V143del, Y144del, Y145del, N211del,L212I, ins214EPE, G339D, S371L,

412   S373P, S375F, K417N, N440K, G446S, S477N, T478K, E484A, Q493R, G496S, Q498R, N501Y,

413   Y505H, T547K, D614G, H655Y, N679K, P681H, N764K, D796Y, N856K, Q954H, N969K,

414   L981F). The spike genes from SARS-CoV-2 related CoVs (RaTG13_GenBank: QHR63300.2;

415   Pangolin GD_GenBank: QIA48632.1; Pangolin_GX-P2V_ QIQ54048.1), SARS-CoV and related

416   CoVs (SARS-CoV Urbani_ GenBank: AAP13441.1; Frankfurt1_GenBank: BAE93401.1; Civet

19

417   SARS CoV 007/2004 S_ GenBank: AAU04646.1; WIV1_GenBank: KF367457;

418   SHC014_GenBank: KC881005), MERS-CoV EMC_ GenBank: AFS88936), hCoV-HKU1

419   (GenBank: AAT98580.1), hCoV-OC43 (GenBank: AAT84354.1), hCoV-NL63 (GenBank:

420   Q6Q1S2.1) and hCoV-229E (GenBank: AOG74783.1) were synthesized (Genscript). These full-

421   length spike plasmids were used for pseudovirus production and for cell surface binding assays.

422

423   **Analysis of WS6 binding to cell surface expressed spike protein**

424   Expi-293 cells were transiently transfected with plasmids encoding full-length spike proteins of

425   coronaviruses using Turbo293 transfection reagent (Speed BioSystems) following manufacturer's

426   protocol. After 40 hours, cells were harvested and incubated with monoclonal antibodies (1 µg/ml)

427   for 30 minutes. Cells were washed and incubated with an allophycocyanin conjugated anti-human

428   IgG (709-136-149, Jackson Immunoresearch Laboratories) for another 30 minutes, then washed

429   and fixed with 1% paraformaldehyde (15712-S, Electron Microscopy Sciences). Flow cytometry

430   data were acquired in a BD LSRFortessa X-50 flow cytometer (BD biosciences) and analyzed

431   using Flowjo (BD biosciences).

432

433   **Pseudovirus neutralization assay**

434   Spike-containing lentiviral pseudovirions were produced by co-transfection of packaging plasmid

435   pCMVdR8.2, transducing plasmid pHR' CMV-Luc, a TMPRSS2 plasmid and S plasmids from

436   human and animal coronaviruses (SARS-CoV-2 variants, SARS-CoV, MERS-CoV and SARS-

437   CoV-2, SARS-CoV related coronaviruses) into 293T cells using Lipofectamine 3000 transfection

438   reagent (L3000-001, ThermoFisher Scientific, Asheville, NC) (Naldini et al., 1996). 293T-ACE2

439   cells (provided by Dr. Michael Farzan) or 293 flpin-TMPRSS2-ACE2 cells (made at the VRC)

20

440   were plated into 96-well white/black Isoplates (PerkinElmer, Waltham, MA) at 75,00 cells per

441   well the day before infection of pseudovirus. Serial dilutions of mAbs were mixed with titrated

442   pseudovirus, incubated for 45 minutes at 37°C and added to cells in triplicate. Following 2 h of

443   incubation, wells were replenished with 150 ml of fresh media. Cells were lysed 72 h later, and

444   luciferase activity was measured with Microbeta (Perking Elmer). Percent neutralization and

445   neutralization IC50s, IC80s were calculated using GraphPad Prism 8.0.2.

446

447   **Neutralization by fusion inhibition (post attachment inhibition)**

448   BHK21-ACE2 or 293 flpin-TMPRSS2-ACE2 cells were placed on ice for one hour before

449   incubating with SARS-CoV-2 spike pseudotyped lentivirus on ice for another hour to allow the virus

450   to attach to ACE2. After 3 times of wash the cells were then incubated with mAbs on ice for

451   additional one hour before returned to the incubator. Cells were lysed 72 h later, and luciferase

452   activity was measured with Microbeta (Perking Elmer). Percent neutralization and neutralization

453   IC50s, IC80s were calculated using GraphPad Prism 8.0.2.

454

455   **Biolayer interferometry analysis of antibody binding affinity**

456   Binding kinetics of WS6 IgG and related S2-stem helix antibodies to diverse CoV 2P-stabilized

457   spike proteins (S2Ps) were measured by biolayer interferometry using an Octet HTX instrument

458   (Sartorius). All assays were performed in tilted 384-well plates (Geiger Bio-one) in HBS-EP+

459   buffer with agitation set to 1000 rpm at 30°C. The final volume for all solutions was 60-80 µl/well.

460   Prior to running the assays, Anti Mouse Fc (AMC) biosensor tips were equilibrated in PBS for ~5

461   minutes. WS6 antibody IgG at 10 µg/ml were loaded onto AMC biosensors for 60s. Biosensors

462   were then equilibrated in HBS-EP+ buffer for 60s prior to measuring association with diverse beta-

463   CoV S2P trimers in solution (0.0019 µM to 0.5µM) for 300s; trimer proteins were then allowed to

464   dissociate for 600s. Parallel correction to subtract systematic baseline drift was carried out by

465   subtracting the measurements recorded for a sensor loaded with antibody incubated in HBS-EP+

466   buffer. Data analysis and curve fitting were carried out using Octet analysis software, version 12.0

467   (Sartorius). Experimental data were fitted using a 1:1 interaction to determine apparent

468   dissociation constants and k_{on} values.

469

470   **Crystallization and structure determination**

471   The N-terminal acetylated, C-terminal biotin-pegylated, 10-residue SARS-CoV-2 S2 peptide

472   FKEELDKYFK (GenScript) was dissolved in 100% DMSO at 10 mg/mL and then diluted with

473   PBS to 1 mg/mL. Fab WS6 was incubated with the peptide in a 1:2 molar ratio for 5 minutes to

474   form complex. The Fab-peptide complex was concentrated to 10-15 mg/mL and screened for

475   crystallization using 576 conditions from Hampton screen, Precipitant Synergy screen, and

476   QIAGEN Wizard screen with a Mosquito robot mixing 100 nL reservoir solution and 100 nL

477   protein solution per drop. Crystals were obtained from the solution containing 2% v/v PEG 400, 2

478   M $(NH_4)_2SO_4$, 100 mM sodium acetate pH 5.5. Crystal drops were set up in 15-well plates using

479   0.5 µL WS6-peptide complex and 0.5 µL of 80-100% concentration of the aforementioned

480   crystallization solution. Crystals were cryoprotected in the aforementioned solution supplemented

481   with 50% additional precipitant and 15% v/v (2R,3R)-2,3-Butanediol and flash frozen in liquid

482   nitrogen.

483   X-ray diffraction data were collected at the Advanced Photon Source (beamline SER-CAT

484   ID22 and BM22). The diffraction data were indexed, integrated, and scaled with the HKL2000

485   package (Otwinowski and Minor, 1997). The structures were determined by molecular

486   replacement with Phaser (McCoy et al., 2007) in the CCP4 Program Suite (Collaborative

487   Computational Project, 1994). Further refinement was carried out with PHENIX (Adams et al.,

488   2010), starting with torsion-angle simulated annealing with slow cooling. Iterative manual model

489   building was carried out with COOT (Emsley and Cowtan, 2004) with maps generated from

490   combinations of standard positional, individual B-factor and TLS refinement algorithms. X-ray

491   data and refinement statistics are summarized in Table S2.

492

493   **Antibody germline assignment**

494   Germline gene of heavy and light chain were assigned by querying nucleotide sequences on

495   IGBLAST server. B6 heavy and light chain germline gene were assigned by submitting protein

496   sequence. The V gene identity was reported as the identity to the germline nucleotide sequences.

497

498   **Antibody frequency calculation**

499   The mouse Ig deep sequencing samples were prepared and used to predict probability of

500   generation of specific protein sequences on CDR3. Human Ig deep sequencing samples were

501   downloaded from Bioproject PRJNA511481. The Ig sequences were sieved for IGOR to inference

502   the model (Marcou et al., 2018). The inferenced models were used by OLGA to predict probability

503   of having specific CDR3 sequences (Sethna et al., 2019). Signature of CV3-25 class antibody was

504   defined as heavy chain IGHV5-51 and light chain IGKV1-12 germline gene, the R94, 96PQYC,

505   G100b, C100d, and W100g on 18 amino acids CDR H3. The frequency of S2P6 class antibody

506   was calculated by defining signature as IGHV1-46 germline gene with 97PKG in 11 amino acids

507   CDR H3, and IGKV3-20 with Y91, 93SSPP and 96F on 11 amino acids CDR L3. The frequency

508   of cc40.8 class antibody was calculated by masking IGHV3-23 with 94ITMA, 101V and 102V on

509   8 amino acids CDR H3 and IGLV3-10 with T91, 94SGN, and A96 on 11 amino acids CDR L3.

510   The frequency of WS6 class antibody calculated by using mouse IGHV1-5 gene with 95TGS on 7

511   amino acids CDR H3, and IGKV4-61 gene with 91Y, 94Y and 96P on 9 amino acids CDR L3. B6

512   and IgG22 used identical heavy chain germline gene, although the light chain used different

513   germline genes, it shared similar contact residues. B6/IgG22 class frequency was calculated by

514   IGHV1-19 germline gene with CX{5,10}RX{4,6}W signature on CDR H3 amino acids, and

515   IGKV8-27 /IGKV1-99 germline genes with 92[LN] and 95[FY] on 8 amino acids length CDR L3.

516

517   **Phylogenetic tree**

518   Alpha-coronavirus spike sequences were downloaded using accession codes (NL63:Q6Q1S2.1,

519   229E:AOG74783.1, Feline:AAY32596.1, Mink:ADI80513.1). Beta-coronavirus spike sequences

520   were downloaded from NCBI server using accession codes listed in Full-length spike constructs.

521   ClustalW was used to calculate neighbor joining (NJ) tree (Larkin et al., 2007), and Dendroscope

522   was used to plot the Neighbor Joining tree (Albrecht et al., 2012).

523

524   **QUANTIFICATION AND STATISTICAL ANALYSIS**

525   The BLI data were analyzed and plotted using GraphPad Prism. Crystal diffraction data

526   and structural refinement statistics were analyzed with HKL2000, Phenix, and Molprobity.

527   Statistical details of experiments are described in Method Details or figure legends.

528

529

References

Adams, P.D., Afonine, P.V., Bunkoczi, G., Chen, V.B., Davis, I.W., Echols, N., Headd, J.J., Hung, L.W., Kapral, G.J., Grosse-Kunstleve, R.W.*, et al.* (2010). PHENIX: a comprehensive Python-based system for macromolecular structure solution. Acta Crystallogr D Biol Crystallogr *66*, 213-21.

Albrecht, B., Scornavacca, C., Cenci, A., and Huson, D.H. (2012). Fast computation of minimum hybridization networks. Bioinformatics *28*, 191-7.

Araf, Y., Akter, F., Tang, Y.D., Fatemi, R., Parvez, S.A., Zheng, C., and Hossain, G. (2022). Omicron variant of SARS-CoV-2: Genomics, transmissibility, and responses to current COVID-19 vaccines. J Med Virol, 10.1002/jmv.27588.

Barnes, C.O., West, A.P., Jr., Huey-Tubman, K.E., Hoffmann, M.A.G., Sharaf, N.G., Hoffman, P.R., Koranda, N., Gristick, H.B., Gaebler, C., Muecksch, F.*, et al.* (2020). Structures of Human Antibodies Bound to SARS-CoV-2 Spike Reveal Common Epitopes and Recurrent Features of Antibodies. Cell *182*, 828-842 e16.

Barouch, D.H., Yang, Z.Y., Kong, W.P., Korioth-Schmitz, B., Sumida, S.M., Truitt, D.M., Kishko, M.G., Arthur, J.C., Miura, A., Mascola, J.R.*, et al.* (2005). A human T-cell leukemia virus type 1 regulatory element enhances the immunogenicity of human immunodeficiency virus type 1 DNA vaccines in mice and nonhuman primates. J Virol *79*, 8828-34.

Boyoglu-Barnum, S., Ellis, D., Gillespie, R.A., Hutchinson, G.B., Park, Y.J., Moin, S.M., Acton, O.J., Ravichandran, R., Murphy, M., Pettie, D.*, et al.* (2021). Quadrivalent influenza nanoparticle vaccines induce broad protection. Nature *592*, 623-628.

Brouwer, P.J.M., Caniels, T.G., van der Straten, K., Snitselaar, J.L., Aldon, Y., Bangaru, S., Torres, J.L., Okba, N.M.A., Claireaux, M., Kerster, G.*, et al.* (2020). Potent neutralizing antibodies from COVID-19 patients define multiple targets of vulnerability. Science *369*, 643-650.

Cai, Y., Zhang, J., Xiao, T., Peng, H., Sterling, S.M., Walsh, R.M., Rawson, S., Rits-Volloch, S., and Chen, B. (2020). Distinct conformational states of SARS-CoV-2 spike protein. Science, eabd4251.

Cao, Y., Su, B., Guo, X., Sun, W., Deng, Y., Bao, L., Zhu, Q., Zhang, X., Zheng, Y., Geng, C.*, et al.* (2020). Potent neutralizing antibodies against SARS-CoV-2 identified by high-throughput single-cell sequencing of convalescent patients' B cells. Cell, 10.1016/j.cell.2020.05.025.

Cerutti, G., Guo, Y., Zhou, T., Gorman, J., Lee, M., Rapp, M., Reddem, E.R., Yu, J., Bahna, F., Bimela, J.*, et al.* (2021). Potent SARS-CoV-2 neutralizing antibodies directed against spike N-terminal domain target a single supersite. Cell Host Microbe *29*, 819-833 e7.

Collaborative Computational Project, N. (1994). The CCP4 suite: programs for protein crystallography. Acta Crystallogr D Biol Crystallogr *50*, 760-3.

565 Corbett, K.S., Edwards, D.K., Leist, S.R., Abiona, O.M., Boyoglu-Barnum, S., Gillespie, R.A.,
566 Himansu, S., Schafer, A., Ziwawo, C.T., DiPiazza, A.T.*, et al.* (2020). SARS-CoV-2 mRNA
567 vaccine design enabled by prototype pathogen preparedness. Nature *586*, 567-571.

568 Doria-Rose, N.A., Shen, X., Schmidt, S.D., O'Dell, S., McDanal, C., Feng, W., Tong, J., Eaton, A.,
569 Maglinao, M., Tang, H.*, et al.* (2021). Booster of mRNA-1273 Strengthens SARS-CoV-2 Omicron
570 Neutralization. medRxiv, 10.1101/2021.12.15.21267805.

571 Drosten, C., Gunther, S., Preiser, W., van der Werf, S., Brodt, H.R., Becker, S., Rabenau, H.,
572 Panning, M., Kolesnikova, L., Fouchier, R.A.*, et al.* (2003). Identification of a novel coronavirus
573 in patients with severe acute respiratory syndrome. N Engl J Med *348*, 1967-76.

574 Edara, V.V., Manning, K.E., Ellis, M., Lai, L., Moore, K.M., Foster, S.L., Floyd, K., Davis-
575 Gardner, M.E., Mantus, G., Nyhoff, L.E.*, et al.* (2021). mRNA-1273 and BNT162b2 mRNA
576 vaccines have reduced neutralizing activity against the SARS-CoV-2 Omicron variant. bioRxiv,
577 10.1101/2021.12.20.473557.

578 Emsley, P., and Cowtan, K. (2004). Coot: model-building tools for molecular graphics. Acta
579 Crystallogr D Biol Crystallogr *60*, 2126-32.

580 Garcia-Beltran, W.F., St Denis, K.J., Hoelzemer, A., Lam, E.C., Nitido, A.D., Sheehan, M.L.,
581 Berrios, C., Ofoman, O., Chang, C.C., Hauser, B.M.*, et al.* (2022). mRNA-based COVID-19
582 vaccine boosters induce neutralizing immunity against SARS-CoV-2 Omicron variant. Cell,
583 10.1016/j.cell.2021.12.033.

584 Hsieh, C.L., Werner, A.P., Leist, S.R., Stevens, L.J., Falconer, E., Goldsmith, J.A., Chou, C.W.,
585 Abiona, O.M., West, A., Westendorf, K.*, et al.* (2021). Stabilized coronavirus spike stem elicits a
586 broadly protective antibody. Cell Rep *37*, 109929.

587 Ju, B., Zhang, Q., Ge, J., Wang, R., Sun, J., Ge, X., Yu, J., Shan, S., Zhou, B., Song, S.*, et al.*
588 (2020). Human neutralizing antibodies elicited by SARS-CoV-2 infection. Nature *584*, 115-119.

589 Kanekiyo, M., Wei, C.J., Yassine, H.M., McTamney, P.M., Boyington, J.C., Whittle, J.R., Rao,
590 S.S., Kong, W.P., Wang, L., and Nabel, G.J. (2013). Self-assembling influenza nanoparticle
591 vaccines elicit broadly neutralizing H1N1 antibodies. Nature *499*, 102-6.

592 Ke, Z., Oton, J., Qu, K., Cortese, M., Zila, V., McKeane, L., Nakane, T., Zivanov, J., Neufeldt,
593 C.J., Cerikan, B.*, et al.* (2020). Structures and distributions of SARS-CoV-2 spike proteins on
594 intact virions. Nature *588*, 498-502.

595 Kong, R., Duan, H., Sheng, Z., Xu, K., Acharya, P., Chen, X., Cheng, C., Dingens, A.S., Gorman,
596 J., Sastry, M.*, et al.* (2019). Antibody Lineages with Vaccine-Induced Antigen-Binding Hotspots
597 Develop Broad HIV Neutralization. Cell *178*, 567-584 e19.

598 Kong, R., Xu, K., Zhou, T., Acharya, P., Lemmin, T., Liu, K., Ozorowski, G., Soto, C., Taft, J.D.,
599 Bailer, R.T.*, et al.* (2016). Fusion peptide of HIV-1 as a site of vulnerability to neutralizing
600 antibody. Science *352*, 828-33.

601 Ksiazek, T.G., Erdman, D., Goldsmith, C.S., Zaki, S.R., Peret, T., Emery, S., Tong, S., Urbani, C.,
602 Comer, J.A., Lim, W., *et al.* (2003). A novel coronavirus associated with severe acute respiratory
603 syndrome. N Engl J Med *348*, 1953-66.

604 Larkin, M.A., Blackshields, G., Brown, N.P., Chenna, R., McGettigan, P.A., McWilliam, H.,
605 Valentin, F., Wallace, I.M., Wilm, A., Lopez, R., *et al.* (2007). Clustal W and Clustal X version
606 2.0. Bioinformatics *23*, 2947-8.

607 Li, W., Chen, Y., Prevost, J., Ullah, I., Lu, M., Gong, S.Y., Tauzin, A., Gasser, R., Vezina, D.,
608 Anand, S.P., *et al.* (2022). Structural basis and mode of action for two broadly neutralizing
609 antibodies against SARS-CoV-2 emerging variants of concern. Cell Rep *38*, 110210.

610 Liu, L., Iketani, S., Guo, Y., Chan, J.F., Wang, M., Liu, L., Luo, Y., Chu, H., Huang, Y., Nair,
611 M.S., *et al.* (2021). Striking Antibody Evasion Manifested by the Omicron Variant of SARS-CoV-
612 2. Nature, 2021.12.14.472719.

613 Liu, L., Wang, P., Nair, M.S., Yu, J., Rapp, M., Wang, Q., Luo, Y., Chan, J.F., Sahi, V., Figueroa,
614 A., *et al.* (2020). Potent neutralizing antibodies against multiple epitopes on SARS-CoV-2 spike.
615 Nature *584*, 450-456.

616 Marcou, Q., Mora, T., and Walczak, A.M. (2018). High-throughput immune repertoire analysis
617 with IGoR. Nat Commun *9*, 561.

618 McCallum, M., De Marco, A., Lempp, F.A., Tortorici, M.A., Pinto, D., Walls, A.C., Beltramello,
619 M., Chen, A., Liu, Z., Zatta, F., *et al.* (2021). N-terminal domain antigenic mapping reveals a site
620 of vulnerability for SARS-CoV-2. Cell *184*, 2332-2347 e16.

621 McCoy, A.J., Grosse-Kunstleve, R.W., Adams, P.D., Winn, M.D., Storoni, L.C., and Read, R.J.
622 (2007). Phaser crystallographic software. J Appl Crystallogr *40*, 658-674.

623 Naldini, L., Blomer, U., Gage, F.H., Trono, D., and Verma, I.M. (1996). Efficient transfer,
624 integration, and sustained long-term expression of the transgene in adult rat brains injected with a
625 lentiviral vector. Proc Natl Acad Sci U S A *93*, 11382-8.

626 Otwinowski, Z., and Minor, W. (1997). Processing of X-ray diffraction data collected in oscillation
627 mode. Methods Enzymol *276*, 307-26.

628 Pinto, D., Sauer, M.M., Czudnochowski, N., Low, J.S., Tortorici, M.A., Housley, M.P., Noack, J.,
629 Walls, A.C., Bowen, J.E., Guarino, B., *et al.* (2021). Broad betacoronavirus neutralization by a
630 stem helix-specific human antibody. Science *373*, 1109-1116.

631 Robbiani, D.F., Gaebler, C., Muecksch, F., Lorenzi, J.C.C., Wang, Z., Cho, A., Agudelo, M.,
632 Barnes, C.O., Gazumyan, A., Finkin, S., *et al.* (2020). Convergent antibody responses to SARS-
633 CoV-2 in convalescent individuals. Nature *584*, 437-442.

634 Rogers, T.F., Zhao, F., Huang, D., Beutler, N., Burns, A., He, W.T., Limbo, O., Smith, C., Song,
635 G., Woehl, J., *et al.* (2020). Isolation of potent SARS-CoV-2 neutralizing antibodies and protection
636 from disease in a small animal model. Science *369*, 956-963.

637   Sauer, M.M., Tortorici, M.A., Park, Y.J., Walls, A.C., Homad, L., Acton, O.J., Bowen, J.E., Wang,
638   C., Xiong, X., de van der Schueren, W., *et al.* (2021). Structural basis for broad coronavirus
639   neutralization. Nat Struct Mol Biol *28*, 478-486.

640   Sethna, Z., Elhanati, Y., Callan, C.G., Walczak, A.M., and Mora, T. (2019). OLGA: fast
641   computation of generation probabilities of B- and T-cell receptor amino acid sequences and motifs.
642   Bioinformatics *35*, 2974-2981.

643   Seydoux, E., Homad, L.J., MacCamy, A.J., Parks, K.R., Hurlburt, N.K., Jennewein, M.F., Akins,
644   N.R., Stuart, A.B., Wan, Y.H., Feng, J., *et al.* (2020). Analysis of a SARS-CoV-2-Infected
645   Individual Reveals Development of Potent Neutralizing Antibodies with Limited Somatic
646   Mutation. Immunity *53*, 98-105 e5.

647   Sievers, B.L., Chakraborty, S., Xue, Y., Gelbart, T., Gonzalez, J.C., Cassidy, A.G., Golan, Y.,
648   Prahl, M., Gaw, S.L., Arunachalam, P.S., *et al.* (2022). Antibodies elicited by SARS-CoV-2
649   infection or mRNA vaccines have reduced neutralizing activity against Beta and Omicron
650   pseudoviruses. Sci Transl Med, eabn7842.

651   Suryadevara, N., Shrihari, S., Gilchuk, P., VanBlargan, L.A., Binshtein, E., Zost, S.J., Nargi, R.S.,
652   Sutton, R.E., Winkler, E.S., Chen, E.C., *et al.* (2021). Neutralizing and protective human
653   monoclonal antibodies recognizing the N-terminal domain of the SARS-CoV-2 spike protein. Cell
654   *184*, 2316-2331 e15.

655   Syed, A.M., Ciling, A., Khalid, M.M., Sreekumar, B., Chen, P.Y., Kumar, G.R., Silva, I., Milbes,
656   B., Kojima, N., Hess, V., *et al.* (2022). Omicron mutations enhance infectivity and reduce antibody
657   neutralization of SARS-CoV-2 virus-like particles. medRxiv, 10.1101/2021.12.20.21268048.

658   Wang, L., Zhou, T., Zhang, Y., Yang, E.S., Schramm, C.A., Shi, W., Pegu, A., Oloniniyi, O.K.,
659   Henry, A.R., Darko, S., *et al.* (2021). Ultrapotent antibodies against diverse and highly
660   transmissible SARS-CoV-2 variants. Science *373*, eabh1766.

661   Wrapp, D., Wang, N., Corbett, K.S., Goldsmith, J.A., Hsieh, C.L., Abiona, O., Graham, B.S., and
662   McLellan, J.S. (2020). Cryo-EM structure of the 2019-nCoV spike in the prefusion conformation.
663   Science *367*, 1260-1263.

664   Wu, X., Zhou, T., Zhu, J., Zhang, B., Georgiev, I., Wang, C., Chen, X., Longo, N.S., Louder, M.,
665   McKee, K., *et al.* (2011). Focused evolution of HIV-1 neutralizing antibodies revealed by
666   structures and deep sequencing. Science *333*, 1593-602.

667   Xu, K., Acharya, P., Kong, R., Cheng, C., Chuang, G.Y., Liu, K., Louder, M.K., O'Dell, S., Rawi,
668   R., Sastry, M., *et al.* (2018). Epitope-based vaccine design yields fusion peptide-directed
669   antibodies that neutralize diverse strains of HIV-1. Nat Med *24*, 857-867.

670   Yassine, H.M., Boyington, J.C., McTamney, P.M., Wei, C.J., Kanekiyo, M., Kong, W.P.,
671   Gallagher, J.R., Wang, L., Zhang, Y., Joyce, M.G., *et al.* (2015). Hemagglutinin-stem
672   nanoparticles generate heterosubtypic influenza protection. Nat Med *21*, 1065-70.

673   Zaki, A.M., van Boheemen, S., Bestebroer, T.M., Osterhaus, A.D., and Fouchier, R.A. (2012).
674   Isolation of a novel coronavirus from a man with pneumonia in Saudi Arabia. N Engl J Med *367*,
675   1814-20.

676   Zhou, P., Yang, X.L., Wang, X.G., Hu, B., Zhang, L., Zhang, W., Si, H.R., Zhu, Y., Li, B., Huang,
677   C.L.*, et al.* (2020a). A pneumonia outbreak associated with a new coronavirus of probable bat
678   origin. Nature *579*, 270-273.

679   Zhou, P., Yuan, M., Song, G., Beutler, N., Shaabani, N., Huang, D., He, W.T., Zhu, X., Callaghan,
680   S., Yong, P.*, et al.* (2021). A protective broadly cross-reactive human antibody defines a conserved
681   site of vulnerability on beta-coronavirus spikes. bioRxiv, 10.1101/2021.03.30.437769.

682   Zhou, T., Teng, I.T., Olia, A.S., Cerutti, G., Gorman, J., Nazzari, A., Shi, W., Tsybovsky, Y.,
683   Wang, L., Wang, S.*, et al.* (2020b). Structure-Based Design with Tag-Based Purification and In-
684   Process Biotinylation Enable Streamlined Development of SARS-CoV-2 Spike Molecular Probes.
685   Cell Rep *33*, 108322.

686   Zhu, N., Zhang, D., Wang, W., Li, X., Yang, B., Song, J., Zhao, X., Huang, B., Shi, W., Lu, R.*, et
687   al.* (2020). A Novel Coronavirus from Patients with Pneumonia in China, 2019. N Engl J Med *382*,
688   727-733.

689   Zost, S.J., Gilchuk, P., Chen, R.E., Case, J.B., Reidy, J.X., Trivette, A., Nargi, R.S., Sutton, R.E.,
690   Suryadevara, N., Chen, E.C.*, et al.* (2020). Rapid isolation and profiling of a diverse panel of
691   human monoclonal antibodies targeting the SARS-CoV-2 spike protein. Nat Med *26*, 1422-1427.
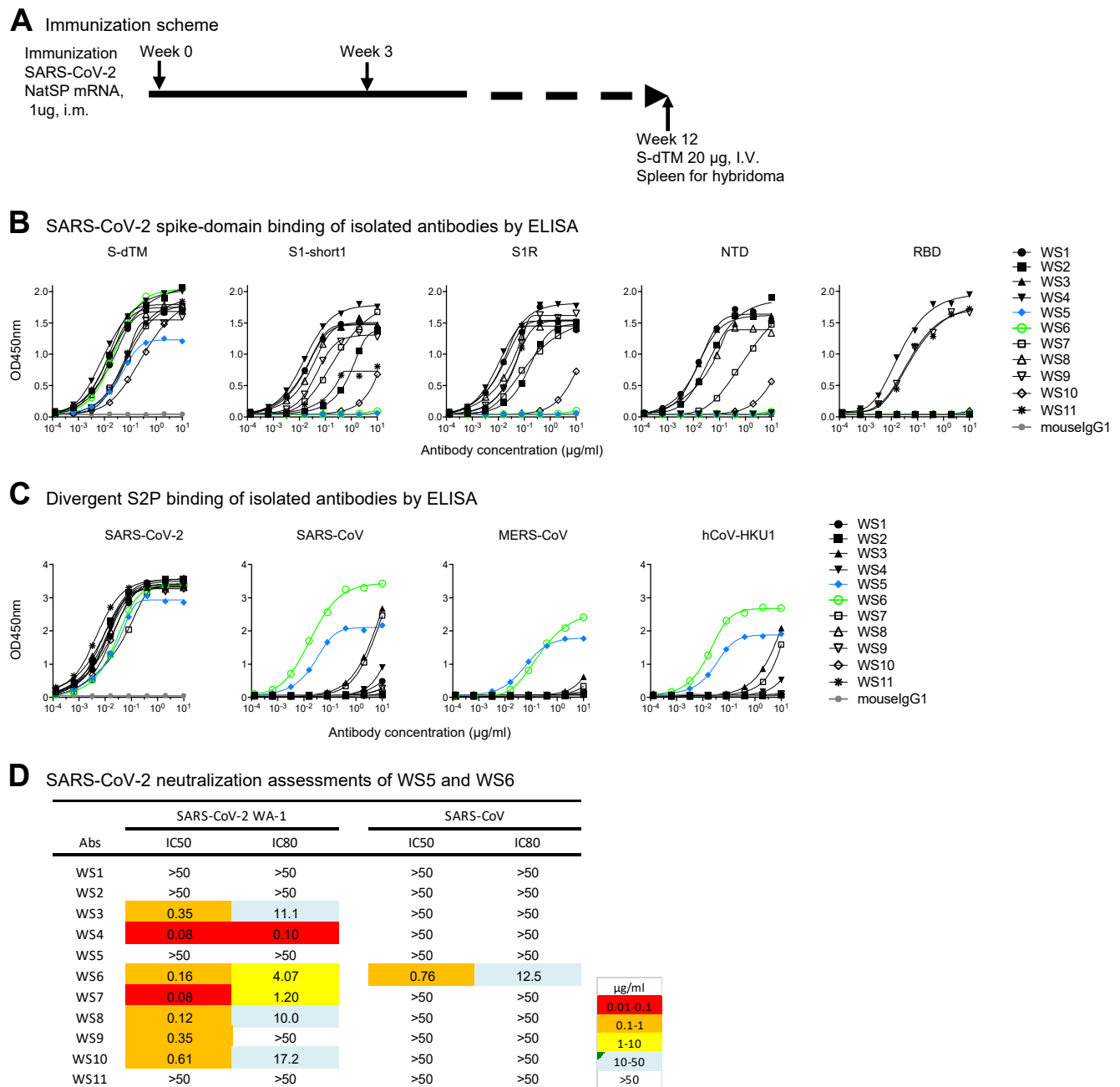
692

Figure 1

Figure 1. Spike mRNA immunized mice elicit antibodies against diverse regions of spike, several of which bound diverse beta-coronavirus spikes and one of which, WS6, neutralized.
(**A**) Immunization scheme. NatSP is the full transmembrane-containing native sequence of spike WA-1 strain; S-dTM is the soluble spike protein residues 1-1206 of wildtype WA-1 strain. (**B**) Binding of isolated antibodies by ELISA to prefusion-stabilized spike (S2P) and its subdomains. Purified monoclonal antibodies from hybridoma supernatants were analyzed for binding to SARS-CoV-2 S-dTM, S1 (S1-short and S1R), RBD and NTD by ELISA. (**C**) Binding of isolated antibodies assess by ELISA to diverse beta-coronavirus prefusion-stabilized spikes (S2P). (**D**) Neutralization assessment of hybridoma antibodies against SARS-CoV-2 WA-1 and SARS-CoV pseudovirus on 293T-ACE2 cells. See also Figure S1.
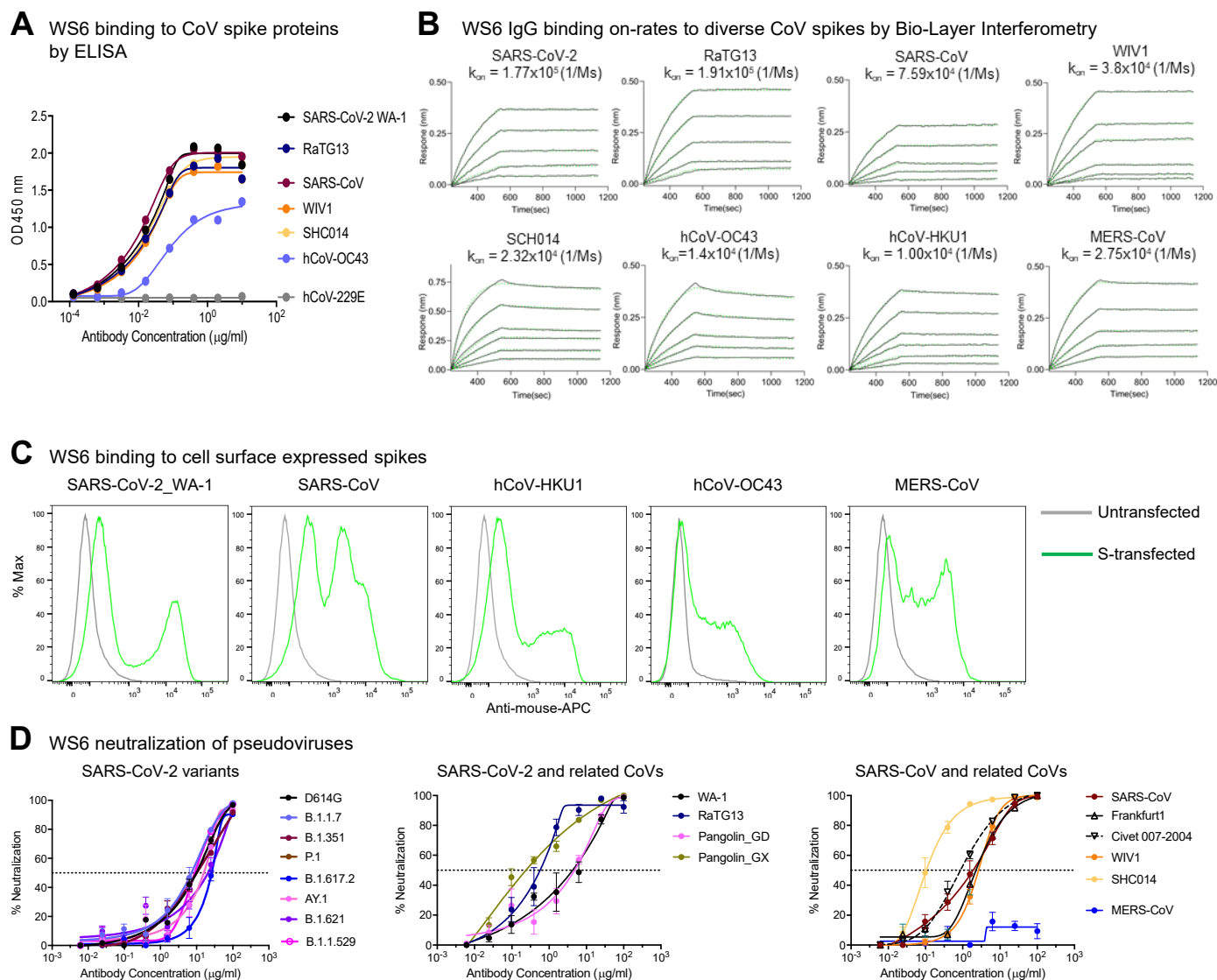
Figure 2

Figure 2. Antibody WS6 binds and neutralizes diverse beta-coronaviruses.
(**A**) ELISA binding analysis of WS6 to prefusion-stabilized soluble spikes of various coronaviruses. (**B**) BLI binding curves of WS6 with various beta-coronaviruses. (**C**) WS6 binds cell surface-expressed spike proteins from SARS-CoV-2, SARS-CoV, hCoV-HKU1, hCoV-OC43 and MERS-CoV. (**D**) WS6 neutralizes SARS-CoV-2 variants, SARS-CoV and related animal coronaviruses. Neutralization activity was measured using spike-pseudotyped lentivirus on 293 flpin-TMPRSS2-ACE2 cells. Assays were performed in triplicate on 293 flpin-TMPRSS2-ACE2 cells, and representative neutralization curves from 2-3 technical replicates are shown. (Left) WS6 neutralizes SARS-CoV-2 variants, D614G, B.1.1.7 (Alpha), B.1.351 (Beta), P.1 (Gamma), B.1.617.2 (Delta), AY.1 (Delta+), B.1.621 (Mu) and B.1.1.529 (Omicron). (Middle) WS6 neutralizes SARS-CoV-2 and related coronaviruses, SARS-CoV-2 WA-1, RaTG13, Pangolin_GD and Pangolin_GX. (Right) WS6 neutralizes SARS-CoV and related coronaviruses, SARS-CoV, Frankfurt1, Civet 007-2004, WIV1 and SHC014, but not MERS-CoV. See also Figure S1, S2, S3 and Table S1.
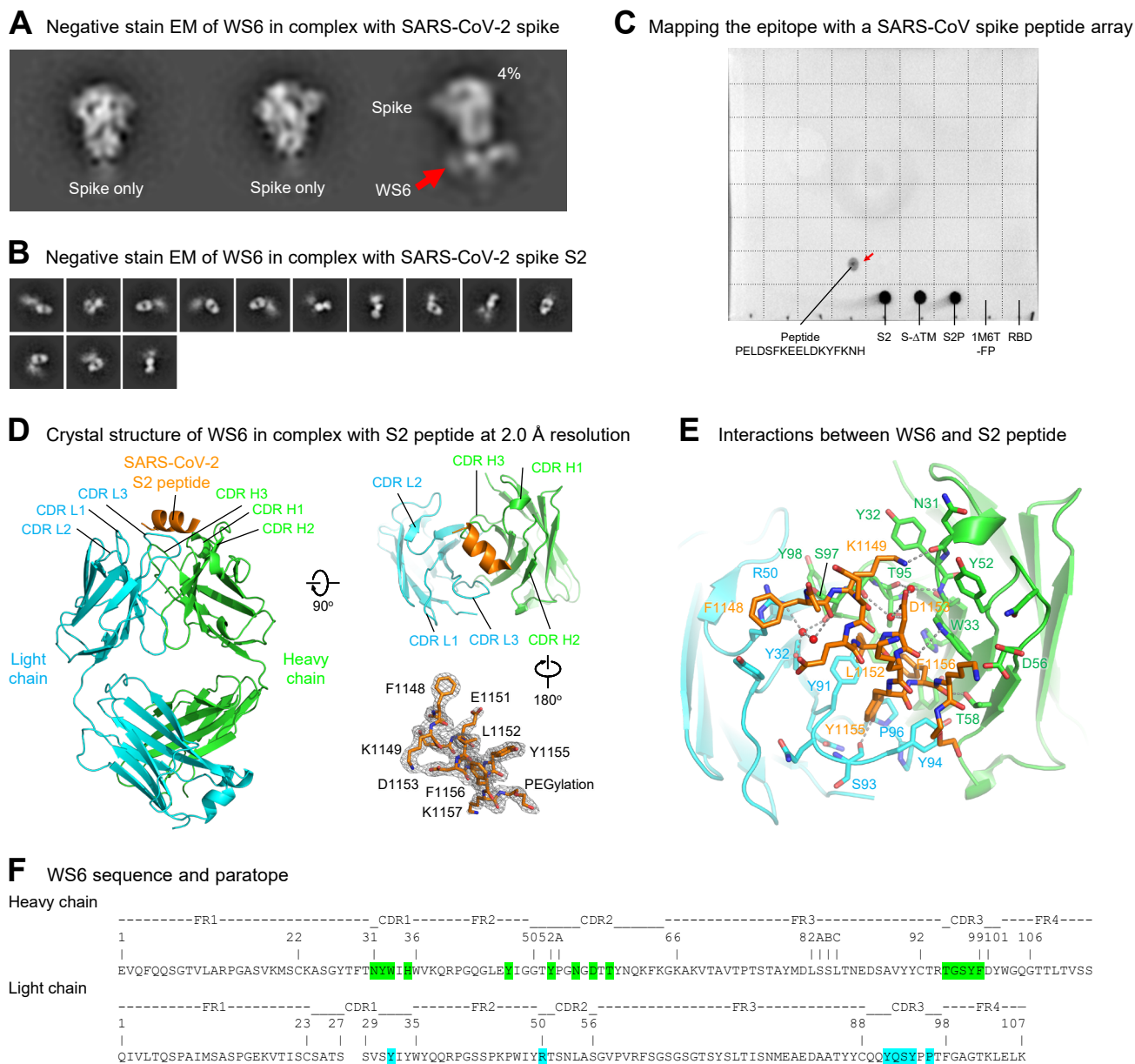
Figure 3

Figure 3. Epitope mapping and crystal structure of antibody WS6 in complex with S2 peptide.
(**A**) Negative stain EM of SARS-CoV-2 spike in complex with WS6. Only a small fraction was observed with WS6 bound at the stem region. (**B**) Negative stain EM of SARS-CoV-2 spike S2 in complex with WS6. (**C**) Epitope mapping by dot-blot assay with a SARS-CoV spike peptide array (BEI, NR-52418). WS6 bound to peptide #154 P_{1125}ELDSFKEELDKYFKNH$_{1141}$ (corresponding to SARS-CoV-2 residues 1143-1159) (red arrow), SARS-CoV-2 spike and its S2 domain. A dash line grid was added on top of the blot to aid display. (**D**) Crystal structure of WS6 in complex with SARS-CoV-2 S2 peptide at 2.0 Å resolution. The antibody and SARS-CoV-2 peptide are shown in cartoon representation. WS6 heavy chain, light chain and S2 peptide are colored green, cyan and orange, respectively. Two 90°-flipped views were shown (left, top right). Electron density map of the S2 peptide was shown with the antibody interacting residues facing the reader (right, bottom) in a 180°-flipped view from panel above. (**E**) Detailed interactions between WS6 and S2 peptide. The S2 peptide and paratope residues in WS6 were shown in sticks representation with other regions of WS6 shown in cartoon representation. Hydrogen bonds were indicated with gray dashed lines. Waters that mediating hydrogen bonds were shown as red spheres. (F) Sequence and paratope of WS6. WS6 residues were numbered according to Kabat nomenclature. Heavy and light chain paratope residues were highlighted in green and cyan, respectively. See also Table S3.
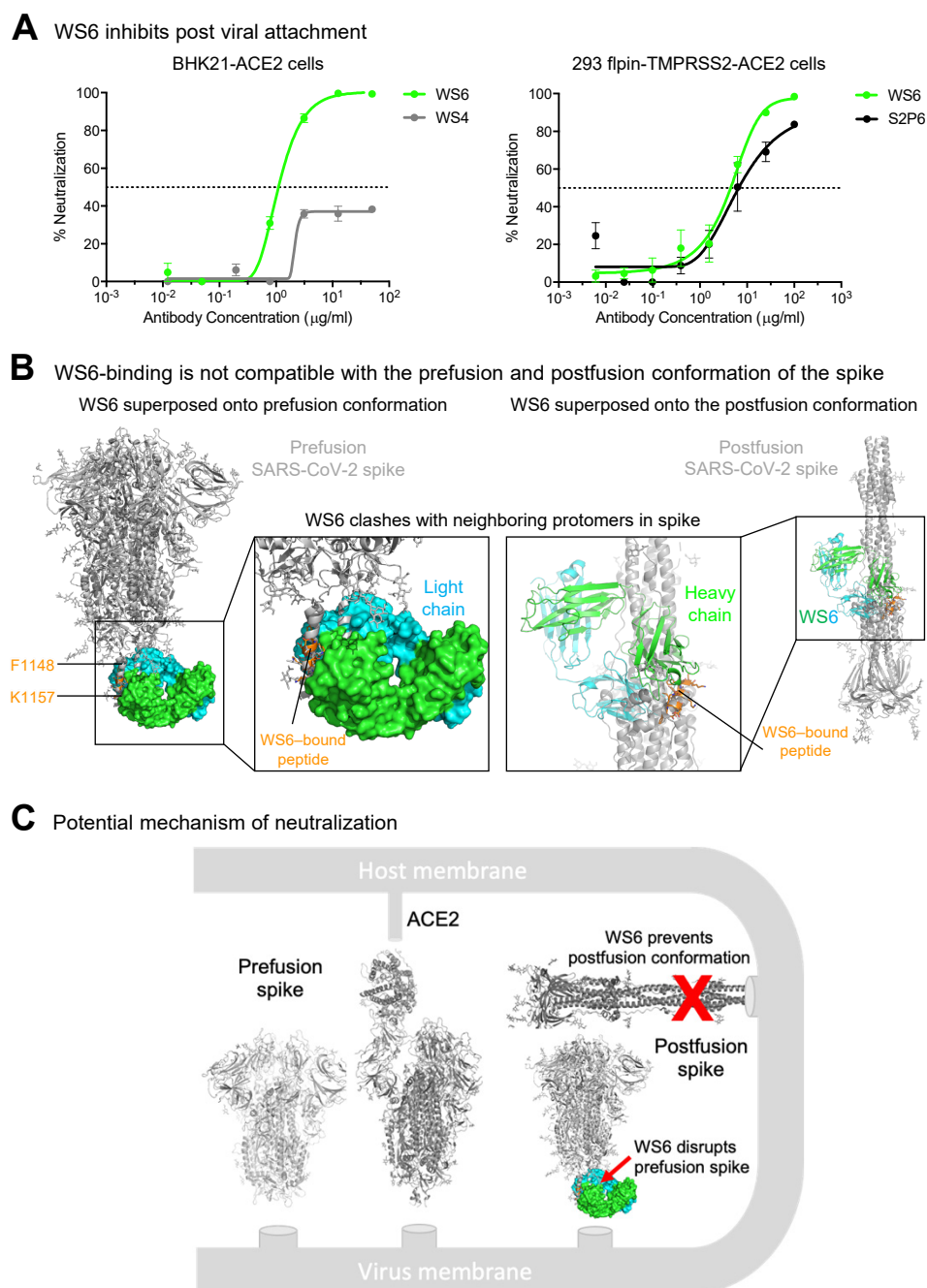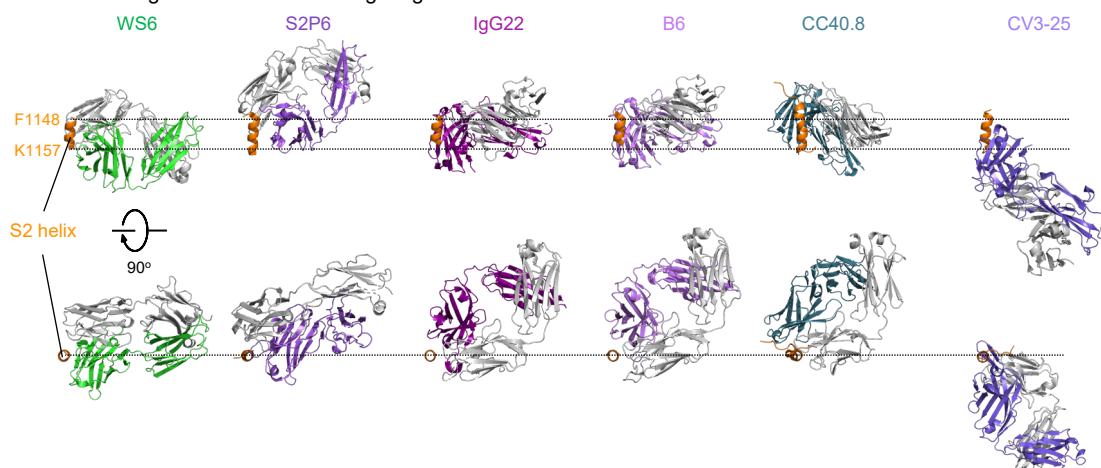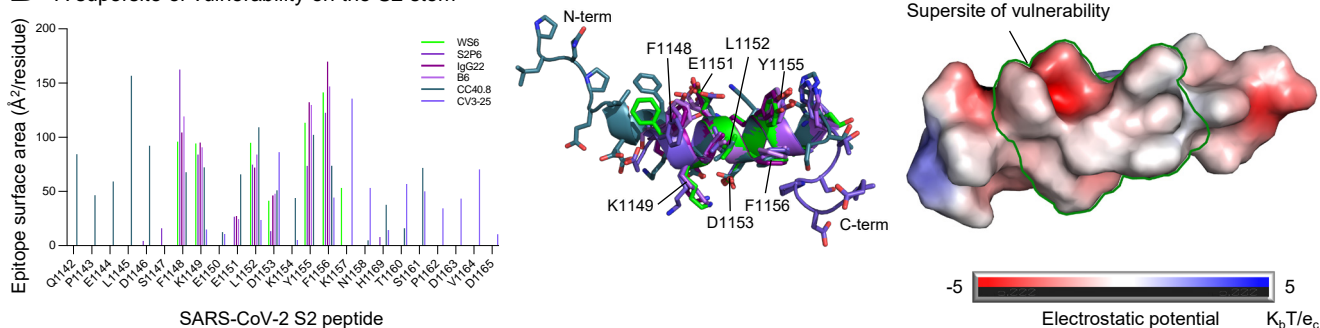
Figure 4

Figure 4. WS6 neutralizes SARS-CoV-2 by inhibition of post viral attachment.
(**A**) WS6 and S2P6 neutralization of SARS-CoV-2 by inhibition of post viral attachment. Neutralization experiments were performed with two BHK21-ACE2 (top) and 293 flpin-TMPRSS2-ACE2 (bottom) cells. WS4, a RBD antibody, was used as a negative control. Representative neutralization curves from two technical replicates of experiments are shown. (**B**) Binding mode of WS6 is not compatible with the prefusion and postfusion conformation of the spike. The WS6-S2 peptide complex was superposed onto the pre- and post-fusion spike trimer by aligning the WS6-bound S2 peptide with the corresponding part in one of the protomers. S2-bound WS6 clashed with neighboring protomers in either prefusion or postfusion conformation, suggesting binding disrupts prefusion conformation and prevents formation of postfusion. (**C**) Mechanism of neutralization by WS6. Structure of WS6 in complex with S2 peptide indicated that WS6 disrupts prefusion spike and prevents formation of the postfusion conformation.

Figure 5

A Comparison of binding orientations of S2-targeting antibodies

B A supersite of vulnerability on the S2 stem

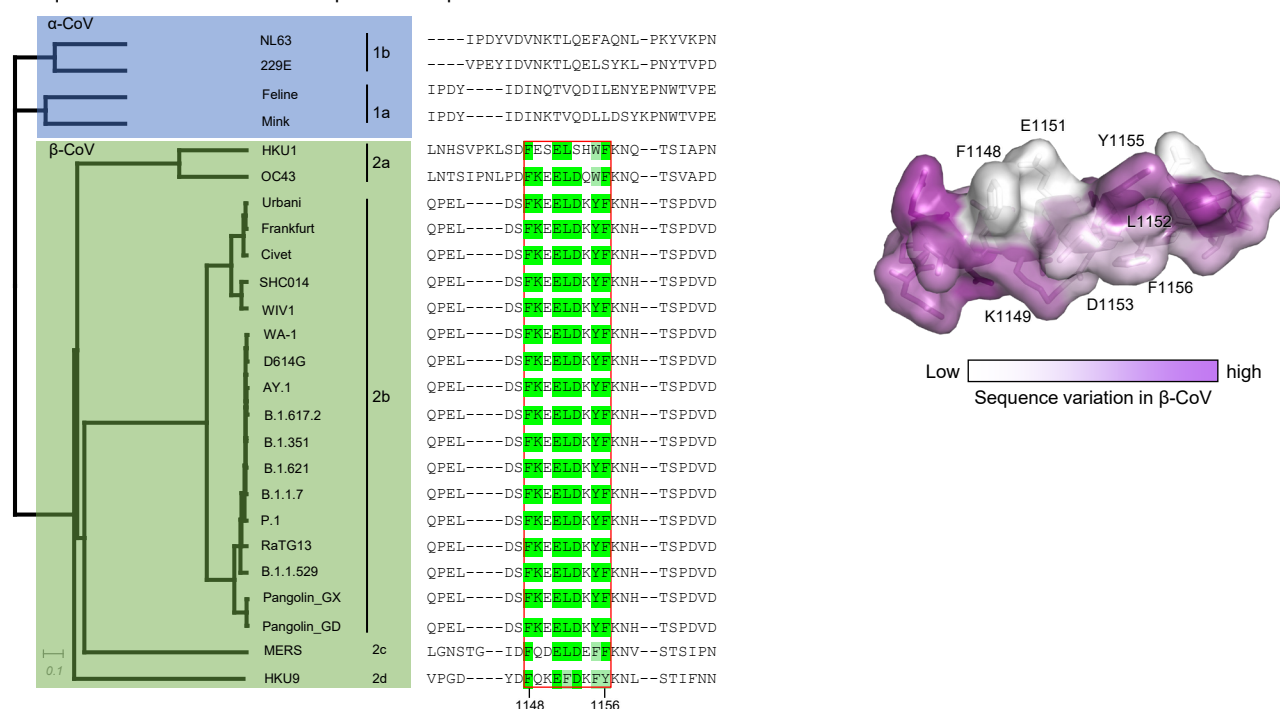**C** Sequence conservation of the supersite in representative beta-coronaviruses

Figure 5. An S2-stem supersite of vulnerability.
(**A**) Comparison of modes of recognition of WS6 with other antibodies targeting the S2 stem helix. WS6 binding to the S2 helix was shown in the same orientation as in Fig. 4B. S2P6, IgG22, B6, CC40.8 and CV3-25 complexes were aligned with the WS6 complex over the S2 peptide helix. The S2 helix and light chains of antibodies were colored orange and gray, respectively. Heavy chains of antibodies are colored differently to distinguish. CV3-25 assumes a distinct mode of recognition comparing to others. (**B**) Epitopes of antibodies targeting the S2 region define a supersite of vulnerability. Antibody-binding surface areas of each residue in the S2 peptide were plotted along the linear sequence of SARS-CoV-2 S2 peptide (left). Antibody-bound peptides were shown colored by recognizing antibodies. The center region between residues 1148 and 1156 were recognized by most of the antibodies (middle), hydrophobic residues F1148, L1152, Y1155 and F1156 were positioned in the middle of the supersite with K1149, E1151 and D1153 providing hydrophilic interactions are the peripheral (right). The boundary of the supersite, which was defined as residues interacting with 5 of the 6 antibodies analyzed in this study, was highlighted by a green line. (**C**) Sequence conservation of the SARS-CoV-2 supersite in β-coronaviruses. Sequence dendrogram was calculated using full spike protein sequences (far left). Sequence alignment shown residues 1142 – 1165, recognized by supersite antibodies in panel B (left middle). The surface of S2 peptide was colored by sequence variation score with corresponding residues shown in sticks representation (right). See also Figures S4 and S5.